

Towards a general parametrization of the warm dark matter halo mass functionMARK R. LOVELL¹¹ *University of Iceland
Dunhaga 5
107 Reykjavík, Iceland*

(Received April 6, 2020; Revised May 28, 2020; Accepted May 31, 2020)

Submitted to ApJ

ABSTRACT

Studies of flux anomalies statistics and perturbations in stellar streams have the potential to constrain models of warm dark matter (WDM), including sterile neutrinos. Producing these constraints requires a parametrization of the WDM mass function relative to that of the cold dark matter (CDM) equivalent. We use five WDM models with half-mode masses, $M_{\text{hm}} = [1.3, 35] \times 10^8 \text{ M}_{\odot}$, spread across simulations of the Local Group, lensing ellipticals and the $z = 2$ universe, to generate such a parametrization: we fit parameters to a functional form for the WDM-to-CDM halo mass function ratio, $n_{\text{WDM}}(M_X)/n_{\text{CDM}}(M_X)$, of $(1 + (\alpha M_{\text{hm}}/M_X)^{\beta})^{\gamma}$. For $M_X \equiv$ virial mass of central halos we obtain $\alpha = 2.3$, $\beta = 0.8$, and $\gamma = -1.0$, and this fit is steeper than the extended Press-Schechter formalism predicts. For $M_X \equiv$ mass of subhalos we instead obtain $\alpha = 4.2$, $\beta = 2.5$ and $\gamma = -0.2$; in both mass definitions the scatter is ~ 20 per cent. The second fit typically underestimates the relative abundance of $z = 2$ WDM subhaloes at the tens of per cent level. We caution that robust constraints will require bespoke simulations and a careful definition of halo mass, particularly for subhalos of mass $< 10^8 \text{ M}_{\odot}$.

Keywords: dark matter:warm dark matter**1. INTRODUCTION**

Recent observations of various astrophysical observables have opened up the possibility of measuring the dark matter halo mass function at redshifts $z < 0.5$. Lensing flux-anomalies studies (Hsueh et al. 2019; Gilman et al. 2019) and an analysis of gaps in stellar streams around the Milky Way (MW) (Banik et al. 2019) have claimed to detect large numbers of dark matter halos at the mass scale of $10^8 - 10^9 \text{ M}_{\odot}$. These analyses then offer the opportunity to place constraints on the presence, or otherwise, of a cut-off in the linear matter power spectrum. The result then provides information about which set of models the dark matter particle can be drawn from. If the dark matter particle belongs to the cold dark matter (CDM) family of candidates such as weakly interacting massive

particles (WIMPs; Ellis et al. 1984) and QCD axions (Turner & Wilczek 1991), then there will be no cut-off at wavenumbers $k < 100 \text{ h/Mpc}$. If instead there is a cut-off in this wavenumber range, this would suggest the dark matter particle is from the warm dark matter (WDM) family of candidates, such as sterile neutrinos (Dodelson & Widrow 1994; Shi & Fuller 1999; Laine & Shaposhnikov 2008; Lovell et al. 2016) or possibly gravitinos (Pagels & Primack 1982).

The crucial step for comparing observational results to dark matter models is an accurate prediction for the halo mass function in each model. Parametrizing the CDM halo mass function is now a well established practice. In its simplest form it is set by the cosmological parameters and the statistics of the pre-galaxy formation epoch density field (Jenkins et al. 2001; Sheth et al. 2001; Ludlow et al. 2016), although baryon physics introduces very significant uncertainty, for example through the ejection of gas (Despali & Vegetti 2017) or through destruction by the disk of the central

galaxy (Garrison-Kimmel et al. 2017). The WDM case has proved much more challenging, for two reasons. First, WDM differs from CDM in that it constitutes a set of cosmologically distinct models, and the rich phenomenology of the sterile neutrino power spectra exhibits a wide variety of cut-off shapes and slopes (Boyarsky et al. 2009; Schneider 2015; Lovell et al. 2016). Second, WDM N -body simulations suffer from the spurious fragmentation of filaments, which generates many more halos than the physical model would predict (Wang & White 2007; Lovell et al. 2014). Methods have been developed to prevent this spurious fragmentation, including using the full six dimensional phase space information (Angulo et al. 2013) and adaptive softening (Hobbs et al. 2016). However most CDM simulations are run with standard N -body solvers, and their WDM counterparts are run with the same code; therefore, methods have to be developed to identify and remove spurious subhaloes in postprocessing (Lovell et al. 2014)¹.

The standard approach to the parametrization of the WDM halo mass function has been to multiply the CDM mass function by a WDM fitting function, R_{fit} , as derived from comparing CDM and WDM simulations of the same volume, i.e.:

$$R_{\text{fit}} = \frac{dN_{\text{WDM}}}{d\log M_X} / \frac{dN_{\text{CDM}}}{d\log M_X} \equiv n_{\text{WDM}}/n_{\text{CDM}}, \quad (1)$$

where N_{WDM} and N_{CDM} are the number of WDM and CDM haloes respectively in each logarithmic mass bin for a given halo mass definition, M_X , and n_{WDM} and n_{CDM} are the differential halo mass functions; note that some studies instead use a more general n_{CDM} derived semi-analytically (Giocoli et al. 2010; Despali & Vegetti 2017). These include the fit to halos in a cosmological box by Schneider et al. (2012), and the fit to subhalos of a MW-analog halo reported by Lovell et al. (2014). Both of these early studies had drawbacks: Schneider et al. (2012) did not consider subhalos; Lovell et al. (2014) instead used a series of zoomed simulations of just one MW-analog halo, such that it is not clear whether the results could be generalized across many halos, and both studies used WDM models with thermal relic masses < 2.3 keV, which are in strong tension with Milky Way satellite counts (Kennedy et al. 2014; Lovell et al. 2016) and Lyman-

α forest analyses (e.g. Viel et al. 2013; Baur et al. 2016). Lovell (2020) argued that such fits offer a poor approximation to extended Press-Schechter (EPS Press & Schechter 1974; Bond et al. 1991; Benson et al. 2013,) expectations for the mass function. Both fits used variations on the Bode et al. (2001) and Viel et al. (2005) thermal relic power spectra, which have different shapes to the particle physics-motivated sterile neutrino power spectra².

The best method currently available for making such comparisons to observations is to first specify the dark matter model parameters and observable of interest, and then perform N -body/hydrodynamical simulations of this system. This approach was taken for lensing arc analyses by Despali et al. (2020), who used simulations of lensing halos at $z = 0.2$ that featured two distinct sterile neutrino models plus the Lovell et al. (2014) algorithm for removing spurious subhalos. Running high resolution simulations of this sort is computationally expensive, thus it is the exception rather than the rule.

In this study we instead use a wide variety of simulations of different environments and sterile neutrino models to derive approximations for R_{fit} , with separate R_{fit} for centrals/isolated halos on the one hand and for subhalos on the other. The purpose of these fits is to provide a first order understanding of whether a given model is in tension with the observational data: we reiterate that the ability to reject any model with certainty requires bespoke simulations of the sort run by Despali et al. (2020).

This *Paper* is organised as follows. In Section 2 we present the simulations, in Section 3 we present our derived halo mass functions, and in Section 4 we draw our conclusions.

2. SIMULATIONS

The simulations used in this paper are derived from three simulation suites. We use the APOSTLE (which we label AP) WDM simulations presented in Lovell et al. (2017), Lovell et al. (2019b) and Lovell et al. (2020); the lensing halo (LH) simulations of Despali et al. (2020), and a previously unpublished simulation of a WDM 25 Mpc uniform resolution, cosmological box (L25) that was run to $z = 2$. These simulations were derived from CDM counterparts: the AP simulations in Fattahi et al. (2016) and Sawala et al.

¹ It has also been suggested that spurious numerical effects in N -body codes may lead to excessive stripping of subhalos (van den Bosch & Ogiya 2018). This effect would apply to both WDM and CDM, so we assume that it is unlikely to be relevant for the subhalo mass function ratio.

² Schneider (2015) applied a version of the Lovell et al. (2014) algorithm to $z = 5$ simulations of less extreme WDM models, and subsequently fit an EPS model, to which Benito et al. (2020) then fit analytical functions.

Table 1. Table of simulations used in this study. The columns are: simulation set name, number of volumes used in each set, type of dark matter model, parent simulation suite, galaxy formation model, mass of the simulation dark matter particle, final redshift of the simulation, cosmology from which the cosmological parameters were derived, half-mode mass of the dark matter model, and the references to the original papers, which are: (1) Lovell et al. (2019b), (2) Lovell et al. (2020), (3) Lovell et al. (2017), (4) Sawala et al. (2016), (5) Despali et al. (2020) (6) Oppenheimer et al. (2016) and (7) Schaye et al. (2015).

Simulation	N_{vols}	DM model	GF model	Suite	$m_{\text{DM}} [\text{M}_{\odot}]$	z	Cosmology	$M_{\text{hm}} [\text{M}_{\odot}]$	Original paper
AP-LA11	1	LA11	Ref	AP-HR	5×10^4	0	WMAP7	9.2×10^8	(1)
AP-LA9	1	LA9	Ref	AP-HR	5×10^4	0	WMAP7	2.6×10^8	(2)
AP-LA120	6	LA120	Ref	AP-MR	6×10^5	0	WMAP7	3.1×10^9	(3)
AP-LA10	6	LA10	Ref	AP-MR	6×10^5	0	WMAP7	5.3×10^8	(3)
AP-CDM(HR)	1	CDM	Ref	AP-HR	5×10^4	0	WMAP7	N/A	(4)
AP-CDM(MR)	6	CDM	Ref	AP-MR	6×10^5	0	WMAP7	N/A	(4)
LH-LA11	4	LA11	Rec	Lens Halo	2×10^6	0.2	Planck	9.4×10^8	(5)
LH-LA8	4	LA8	Rec	Lens Halo	2×10^6	0.2	Planck	1.3×10^8	(5)
LH-CDM	4	CDM	Rec	Lens Halo	2×10^6	0.2	Planck	N/A	(6)
L25-LA120	1	LA120	Rec	25 Mpc box	1×10^6	2	Planck	3.5×10^9	This work
L25-CDM	1	CDM	Rec	25 Mpc box	1×10^6	2	Planck	N/A	(7)

(2016), the LH simulations from Oppenheimer et al. (2016) and the L25 from Schaye et al. (2015).

All of the simulations were run with a variation of the EAGLE galaxy formation code (Crain et al. 2015; Schaye et al. 2015). This code is a heavily-modified version of the P-GADGET3 code (Springel et al. 2008), and features cooling, star-formation (Schaye & Dalla Vecchia 2008), the growth of black holes (Springel 2005; Rosas-Guevara et al. 2015) and feedback from supernova and active galactic nuclei (Booth & Schaye 2009; Dalla Vecchia & Schaye 2012). The EAGLE model parameters were first calibrated for a simulation with a simulation dark matter particle mass of $9.7 \times 10^6 \text{M}_{\odot}$, and this calibration is known as the REFERENCE (‘Ref’) parameter set. The model was subsequently recalibrated for higher resolution simulations – particle mass $1.0 \times 10^6 \text{M}_{\odot}$ – and is therefore known as the RECALIBRATED (‘Rec’) parameter set. The LH and L25 simulations were performed with the Rec parameters, and the AP simulations were instead all run with the Ref parameters, despite having lower dark matter particle masses than both LH and L25.

The halos were identified with the friends-of-friends (FoF) algorithm and decomposed into subhalos using the SUBFIND code (Springel et al. 2001; Dolag et al. 2009). The largest SUBFIND halo in each FoF halo is defined as the central halo, and all other SUBFIND halos as subhalos / satellites. Spurious subhalos were flagged and removed with the Lagrangian region sphericity method of Lovell et al. (2014), using a sphericity cut $s = 0.2$; note that we do not also apply their cut on halo mass. The AP simulations were performed with the WMAP7 cosmological parameters (Komatsu et al. 2011) whereas the other simulations in-

stead used parameters derived from the first Planck results (Planck Collaboration et al. 2014). The AP (LH) simulations are zoomed simulations, and therefore we only use halos/subhalos that are $< 3 \text{ pMpc}$ ($< 4 \text{ pMpc}$) from the high resolution region’s centre-of-potential, whereas for the L25 simulations we use halos from the entire box.

We use five sterile neutrino models in total. Each model is described by two parameters: a sterile neutrino mass and a lepton asymmetry, L_6 ; see Lovell et al. (2016) for a discussion of these quantities. All five models use a sterile neutrino mass of 7.0 keV. The L_6 applied, in the order of most extreme (smallest wavenumber cut-off, or ‘warmest’) to most like CDM, are: $L_6 = 120$ (labeled LA120), the warmest of any 7 keV sterile neutrino; $L_6 = 11.2$ (LA11), the warmest consistent with the sterile neutrino dark matter decay interpretation of the unexplained 3.55 keV X-ray line (Boyarsky et al. 2014; Bulbul et al. 2014); $L_6 = 10$ (LA10), an intermediate case; $L_6 = 9$ (LA9), the coldest consistent with the 3.55 keV line; and finally $L_6 = 8$ (LA8) which is the coldest of any 7 keV sterile neutrino. The matter power spectra of these five models are shown in fig. 1 of Lovell et al. (2017). Note that the different values of L_6 result in changes to the resulting shape of the linear matter power spectrum as well as the location of the cut-off: the LA120 cut-off is the sharpest, and LA8 is the shallowest out of these lepton asymmetry choices.

The LA120 model was applied in six medium resolution (labeled MR, dark matter particle mass $\sim 6 \times 10^5 \text{M}_{\odot}$) AP volumes and the L25 box; LA11 in one high resolution (HR, dark matter particle mass $5 \times 10^4 \text{M}_{\odot}$) AP volume and four LH volumes; LA10 in six MR AP simulations; LA9 in a single HR AP volume and LA8

in four LH simulations. Based on the resolution study in the Aquarius simulations (Springel et al. 2008), we expect that the halo mass functions are resolved to better than 10 per cent above the mass that corresponds to ~ 100 particles. The important properties of all the simulations used in this paper are included in Table 1.

3. RESULTS

The goal of our analysis is to derive a set of fitting functions to the ratio of the WDM and CDM mass functions, R_{fit} . We adopt the functional form:

$$R_{\text{fit}} = n_{\text{WDM}}/n_{\text{CDM}} = (1 + (\alpha M_{\text{hm}}/M_{\text{x}})^{\beta})^{\gamma}, \quad (2)$$

where M_{x} is the halo mass, for a given halo mass definition, and α , β and γ are three fitting parameters. We chose this functional form to mirror the range of shapes of the input linear matter power spectrum (Lovell et al. 2016): a characteristic cut-off scale (α), an approximate asymptotic power-law slope ($\gamma \times \beta$) and also a shape parameter that governs how quickly the curve transitions from flat to the asymptotic slope (β); this form has also been used by Benito et al. (2020). M_{hm} is the half-mode mass, which is defined as the mass scale that corresponds to the power spectrum wavenumber at which the square root of the ratio of the WDM and CDM power spectra is 0.5. The value of M_{hm} for each simulation is given in Table 1: note that because M_{hm} is sensitive to the cosmological parameters, it can vary by a few per cent between simulations with the same DM model.

We adopt two definitions of halo mass. For central halos we use the virial mass, M_{200} , defined as the mass enclosed within the co-moving radius of overdensity 200 times the critical density required for collapse. For subhalos we instead use the gravitational bound mass as determined by SUBFIND, M_{SUBs} . We obtain separate fits – i.e. separate sets of α , β and γ values – for the two mass definitions.

We fit our parameters with the following algorithm. We compute the function in equation 2 for a series of α , β and γ parameter values and then calculate the logarithm of the ratio between this function and the measured $n_{\text{WDM}}/n_{\text{CDM}}$ functions at halo masses (both definitions) 10^8 , 10^9 , and $10^{10} M_{\odot}$ ³. We then calculate the sum of these ratios across all simulations, such that each DM model is given the same weight. We then select the fitting parameters that minimize this function: given

that these fits are intended to be first order approximations we do not compute their χ^2 values. Finally, we note that the number of haloes / subhaloes in our samples ranges from $\gtrsim 70$ (AP-LA120, volume 1) to > 70000 (L25-CDM).

We start our presentation of the resulting fits for the central halo mass function. We plot the ratios of n_{WDM} and n_{CDM} as a function of M_{200} in Fig. 1.

We obtain a fit that diverges by less than 50 per cent in all of the mass bins $> 10^8 M_{\odot}$ that contain more than ten halos. In lower mass bins, resolution effects in both WDM and CDM simulations are expressed. The parameters of this fit are: $\alpha = 2.3$, $\beta = 0.8$, and $\gamma = -1.0$, for an asymptotic low mass slope of -0.8 . Remarkably, this slope almost exactly cancels the low mass slope determined for CDM subhalos – not host halos – in Despali & Vegetti (2017), and therefore this fit predicts that the WDM halo mass function is approximately flat below the half-mode mass; a similar result was obtained in the study by the phase-space solver code of Angulo et al. (2013). We expect that a sharp cut-off in the halo mass function will occur at halo masses $\ll M_{\text{hm}}$, and determining the location of this cut-off will require a careful analysis of the delay in collapse time of low mass WDM haloes plus the statistics of the primordial density field; Benson et al. (2013) argued that a much sharper cut-off will occur if thermal velocities are taken into account.

Our fit works particularly well for the LA8 and LA9 models, producing agreement better than 20 per cent, whereas LA120 is more challenging. There is a systematic bias for the fit to underestimate the number of LA120 halos at $\sim 10^9 M_{\odot}$ and overestimate it at $\sim 10^8 M_{\odot}$. This suggests that LA120 prefers a steeper fit than the other models, which may reflect the fact that the LA120 linear matter power spectrum cut-off is steeper than those of the other models. These fits are somewhat steeper than the EPS mass functions calculated by Lovell (2020), which was calibrated using the high redshift conditional mass functions of $z = 0$ centrals and is therefore a better match to the subhalo mass function than the isolated halo mass function. There are no conspicuous variations between fits attained in different environments, e.g. Local Groups vs. lensing halos. We repeat this exercise for the SUBFIND bound mass of satellite halos, M_{SUBs} , in Fig. 2.

The parameters obtained for the satellite M_{SUBs} are $\alpha = 4.2$, $\beta = 2.5$ and $\gamma = -0.2$: the asymptotic slope is -0.5 and therefore shallower than for M_{200} ; also, the turnover occurs at lower masses. This picture is consistent with the observation in Bose et al. (2016) that the difference between CDM and WDM increases for later

³ We note that the $10^8 M_{\odot}$ bin is only marginally resolved in the LH and LA25 simulations according to our 100 particle limit. The HR and MR AP simulations are resolved comfortably.

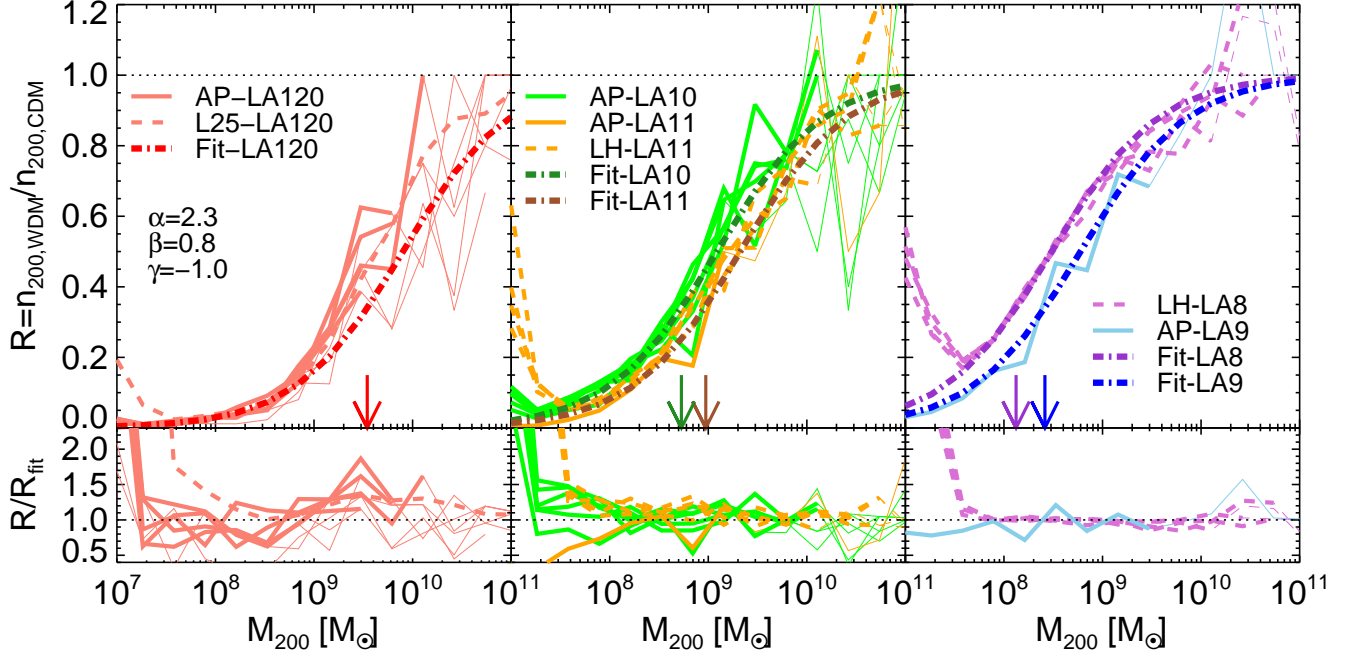


Figure 1. Ratio of WDM to CDM mass functions for central halos using the M_{200} definition of mass. Top panels: the ratio of the WDM mass function to its CDM counterpart for models LA120 (red curves, left-hand panel), LA10 and LA11 (green and orange curves respectively, middle panel), and LA8 and LA9 (purple and blue curves respectively, right-hand panel). In all three panels, the solid curves indicate AP volumes. The dashed curves indicate the L25 box in the left-hand panel and the LH volumes in the other two panels. The fits are shown as dot-dashed curves, with a color darker than the corresponding model: the parameters of the fit are displayed in the left-hand panel. Bottom panels: the ratio of the data curves to the fit. In both sets of panels, curves are drawn thin where each mass bin contains fewer than ten WDM halos and are drawn thick elsewhere. The arrows mark M_{hm} for each of the models: where we use results from both Planck and WMAP7-derived simulations (LA120 and LA11) we plot the arrow using the Planck M_{hm} only.

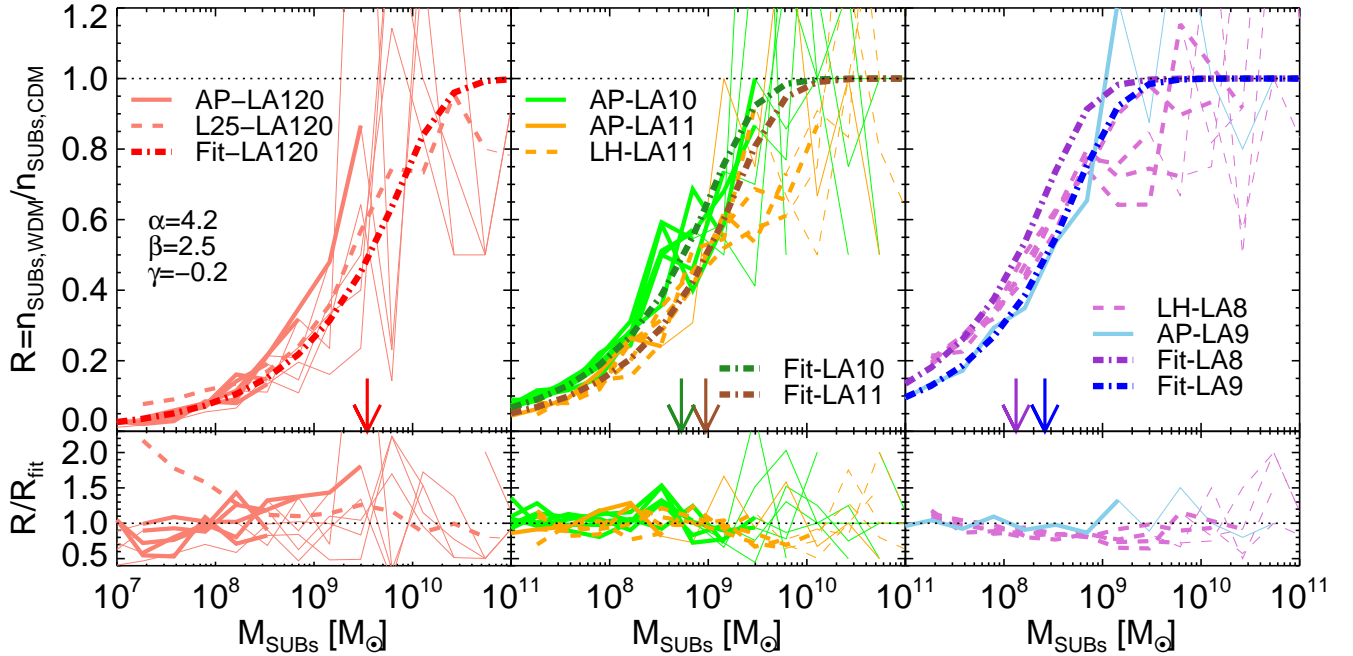


Figure 2. As for Fig. 1, but for subhalos using the SUBFIND bound mass, M_{SUBs} .

forming halos, given that centrals form later than satellites. Another example of this is comparing the $z = 2$ L25 simulation to the AP-LA120 volumes, where the former shows an excess of $10^7 M_\odot$ halos over the latter; we discuss the effect of halo formation time and redshift further in the appendix. In several instances the fit overestimates the abundance of $M_{\text{SUBs}} < 10^8 M_\odot$ halos by ~ 20 per cent, except for LA8 where instead it is $2 \times 10^9 M_\odot$ halos that are underestimated. We stress that this result relies on a particular definition of subhalo mass, and alternative subhalo finders may return very different results (Onions et al. 2012).

4. CONCLUSIONS

In this study we revisited the issue of parametrizing the suppression of the halo mass function in warm dark matter (WDM) relative to cold dark matter (CDM), taking advantage of hydrodynamical simulations at a variety of redshifts – $z = 0, 0.2$ and 2 – and a variety of regimes – the Local Group, lensing ellipticals and a uniform cosmological box – to produce a mass function ratio fit, for the purpose of making first order comparisons between WDM models and observations. We find that the central halo differential mass function (using the virial mass definition, M_{200}) is approximated to typically better than 20 per cent using equation 2 with parameters $\alpha = 2.3$, $\beta = 0.8$, and $\gamma = -1.0$. This fit predicts a WDM halo mass function that is approximately flat for M_{200} less than the half-mode mass, thus we expect to detect some $M_{200} \sim 10^6 M_\odot$ haloes in the WDM cosmology but at a drastically lower rate than in CDM. Performing a fit on the subhalo differential mass function (using the bound subhalo mass definition, M_{SUBs}), with the same functional form, we obtain $\alpha = 4.2$, $\beta = 2.5$ and $\gamma = -0.2$, although the accuracy of this subhalo fit to the simulations is not as consistent as the M_{200} fit. In particular, the M_{SUBs} fit consistently underpredicts the number of WDM haloes relative to CDM at $z = 2$ by ~ 30 per cent: we hypothesise that this is due to the delay in collapse time for WDM haloes leading to greater disparities between CDM and WDM at late times (Lovell et al. 2019a).

These fits are to be understood as first order approximation of each mass function. The simulations assume a particular model of galaxy formation and alternative implementations of feedback could return different results (Despali & Vegetti 2017; Garrison-Kimmel et al. 2017). Fitting the subhalo results is particularly challenging; future studies that invoke general fits such as those presented here will ultimately need to be backed up by bespoke, observables-oriented simulations, will need a clear definition of halo mass, and must take account of the dif-

ferences between halo finders in order to claim definitive constraints on a given dark matter model.

ACKNOWLEDGMENTS

MRL is grateful to the owners of the CDM simulations for their willingness to share their data, and would like to thank Wojtek Hellwing and Jesús Zavala for useful comments on the text. MRL acknowledges support by a Grant of Excellence from the Icelandic Research Fund (grant number 173929). This work used the DiRAC@Durham facility managed by the Institute for Computational Cosmology on behalf of the STFC DiRAC HPC Facility (www.dirac.ac.uk). The equipment was funded by BEIS capital funding via STFC capital grants ST/K00042X/1, ST/P002293/1, ST/R002371/1 and ST/S002502/1, Durham University and STFC operations grant ST/R000832/1. DiRAC is part of the National e-Infrastructure. Part of this work was carried out on the Dutch National e-Infrastructure with the support of SURF Cooperative. This project has also benefited from numerical computations performed at the Interdisciplinary Centre for Mathematical and Computational Modelling (ICM) University of Warsaw under grants #no GA67-15, GA67-16 and G63-3

APPENDIX

In this appendix we show the degree to which the mass function ratios differ between $z = 0$ and $z = 2$. We use the AP simulations, for which we have data at $z = 2$, and make the same selection as for the $z = 0$ data, while keeping a 3 cMpc co-moving aperture around the center of the zoom region. We plot these data together with the $z = 0$ results in Fig. 3 for the M_{200} definition of halo mass. We do not use these AP $z = 2$ data for the purpose of deriving the fitting parameters, either in this appendix or in our main results.

We find that the $z = 2$ mass function ratios are largely well described by the fitting function derived using the other datasets, and the fit is of roughly the same ~ 10 per cent accuracy as for the $z = 0$ results for $M_{200} > 10^8 M_\odot$. The most notable exceptions are LA120 and LA10, where the fit frequently underestimates the number of $z = 2$ haloes, which may be explained in part by poor resolution. We repeat this exercise for the subhalo mass functions in Fig. 4.

The fit systematically underestimates the abundance of $z = 2$ AP haloes around $10^8 M_\odot$ at the tens of per cent level. This result is consistent with the results from the $z = 2$ L25-LA120 run, and again likely shows that the suppression of the WDM halo mass function relative to the CDM equivalent becomes stronger towards lower redshift; we expect this phenomenon is due to the correlation between the halo mass – at fixed redshift – and the

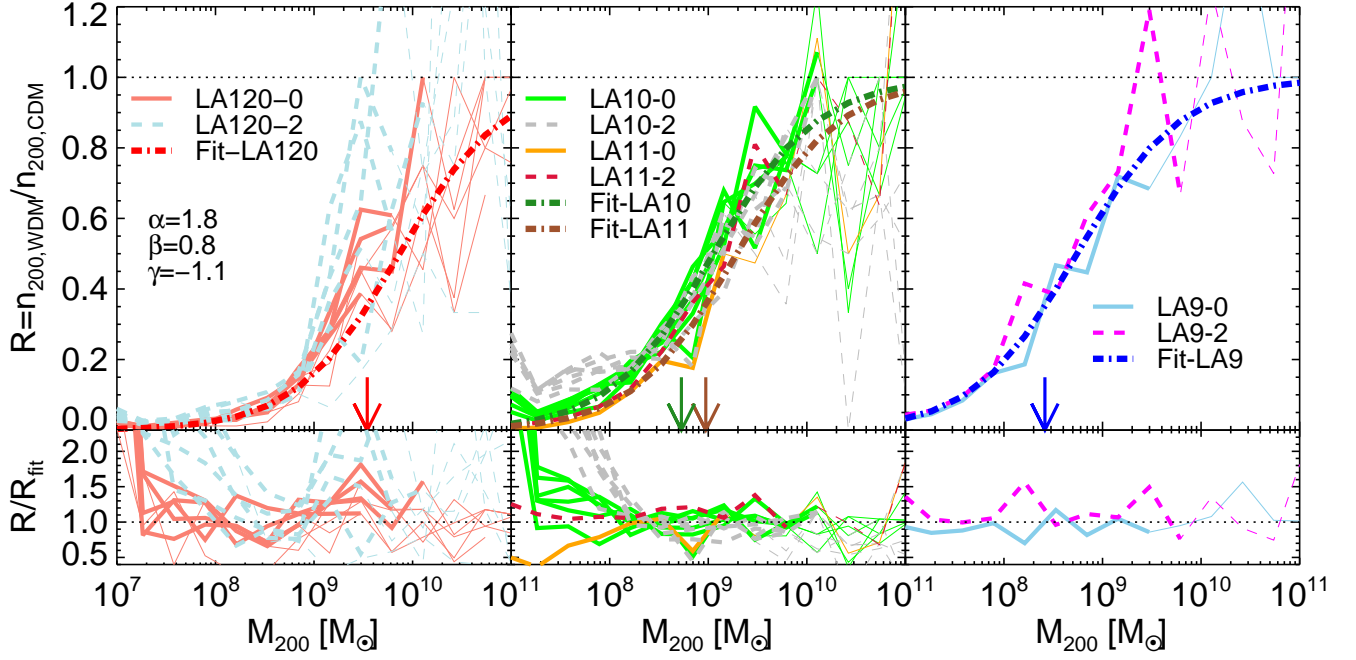


Figure 3. As for Fig. 1, but comparing the M_{200} mass function ratios between the AP $z = 0$ simulations (labeled ‘-0’ in the figure legends), and their $z = 2$ counterparts (labeled ‘-2’). The $z = 2$ data are shown as dashed lines, with their colours as indicated in the figure legends.

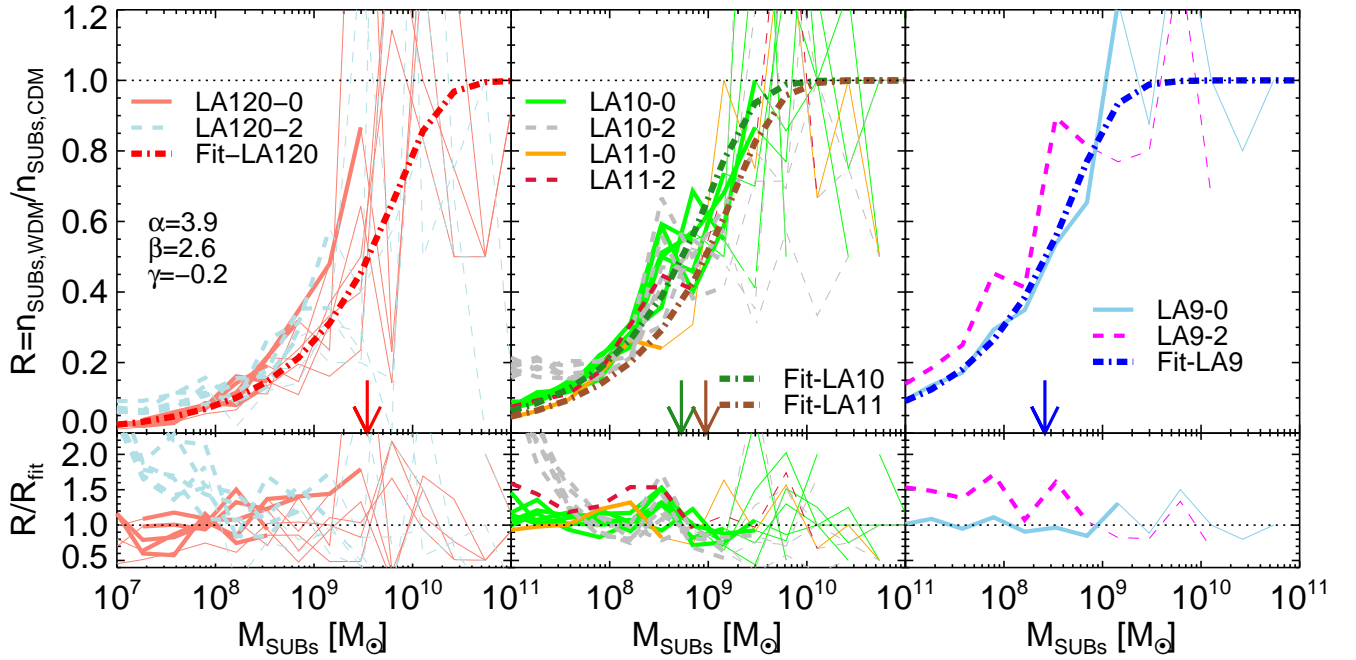


Figure 4. As for Fig. 3, but for subhaloes using the SUBFIND bound mass, M_{SUBs} .

delay in collapse time in WDM simulations (Lovell et al. 2019a). The precise reason for why this effect is stronger

for subhalo M_{SUBs} than for isolated halo M_{200} will be a matter for further study.

REFERENCES

- Angulo, R. E., Hahn, O., & Abel, T. 2013, *MNRAS*, 434, 3337
- Banik, N., Bovy, J., Bertone, G., Erkal, D., & de Boer, T. J. L. 2019, arXiv e-prints, arXiv:1911.02663
- Baur, J., Palanque-Delabrouille, N., Yèche, C., Magneville, C., & Viel, M. 2016, *JCAP*, 2016, 012
- Benito, M., Criado, J. C., Hütsi, G., Raidal, M., & Veermäe, H. 2020, *PhRvD*, 101, 103023
- Benson, A. J., Farahi, A., Cole, S., et al. 2013, *MNRAS*, 428, 1774
- Bode, P., Ostriker, J. P., & Turok, N. 2001, *ApJ*, 556, 93
- Bond, J. R., Cole, S., Efsthathiou, G., & Kaiser, N. 1991, *ApJ*, 379, 440
- Booth, C. M., & Schaye, J. 2009, *MNRAS*, 398, 53
- Bose, S., Hellwing, W. A., Frenk, C. S., et al. 2016, *MNRAS*, 455, 318
- Boyarsky, A., Lesgourgues, J., Ruchayskiy, O., & Viel, M. 2009, *Physical Review Letters*, 102, 201304
- Boyarsky, A., Ruchayskiy, O., Iakubovskiy, D., & Franse, J. 2014, *Physical Review Letters*, 113, 251301
- Bulbul, E., Markevitch, M., Foster, A., et al. 2014, *ApJ*, 789, 13
- Crain, R. A., Schaye, J., Bower, R. G., et al. 2015, *MNRAS*, 450, 1937
- Dalla Vecchia, C., & Schaye, J. 2012, *MNRAS*, 426, 140
- Despali, G., Lovell, M., Vegetti, S., Crain, R. A., & Oppenheimer, B. D. 2020, *MNRAS*, 491, 1295
- Despali, G., & Vegetti, S. 2017, *MNRAS*, 469, 1997
- Dodelson, S., & Widrow, L. M. 1994, *Physical Review Letters*, 72, 17
- Dolag, K., Borgani, S., Murante, G., & Springel, V. 2009, *MNRAS*, 399, 497
- Ellis, J., Hagelin, J. S., Nanopoulos, D. V., Olive, K., & Srednicki, M. 1984, *Nuclear Physics B*, 238, 453
- Fattahi, A., Navarro, J. F., Sawala, T., et al. 2016, *MNRAS*, 457, 844
- Garrison-Kimmel, S., Wetzel, A., Bullock, J. S., et al. 2017, *MNRAS*, 471, 1709
- Gilman, D., Du, X., Benson, A., et al. 2019, *MNRAS*, L167
- Giocoli, C., Tormen, G., Sheth, R. K., & van den Bosch, F. C. 2010, *MNRAS*, 404, 502
- Hobbs, A., Read, J. I., Agertz, O., Iannuzzi, F., & Power, C. 2016, *MNRAS*, 458, 468
- Hsueh, J. W., Enzi, W., Vegetti, S., et al. 2019, *MNRAS*, 2780
- Jenkins, A., Frenk, C. S., White, S. D. M., et al. 2001, *MNRAS*, 321, 372
- Kennedy, R., Frenk, C., Cole, S., & Benson, A. 2014, *MNRAS*, 442, 2487
- Komatsu, E., Smith, K. M., Dunkley, J., et al. 2011, *ApJS*, 192, 18
- Laine, M., & Shaposhnikov, M. 2008, *JCAP*, 6, 31
- Lovell, M. R. 2020, *MNRAS*, 493, L11
- Lovell, M. R., Frenk, C. S., Eke, V. R., et al. 2014, *MNRAS*, 439, 300
- Lovell, M. R., Hellwing, W., Ludlow, A., et al. 2020, arXiv e-prints, arXiv:2002.11129
- Lovell, M. R., Zavala, J., & Vogelsberger, M. 2019a, *MNRAS*, 485, 5474
- Lovell, M. R., Bose, S., Boyarsky, A., et al. 2016, *MNRAS*, 461, 60
- . 2017, *MNRAS*, 468, 4285
- Lovell, M. R., Barnes, D., Bahé, Y., et al. 2019b, *MNRAS*, 485, 4071
- Ludlow, A. D., Bose, S., Angulo, R. E., et al. 2016, *MNRAS*, 460, 1214
- Onions, J., Knebe, A., Pearce, F. R., et al. 2012, *MNRAS*, 423, 1200
- Oppenheimer, B. D., Crain, R. A., Schaye, J., et al. 2016, *MNRAS*, 460, 2157
- Pagels, H., & Primack, J. R. 1982, *PhRvL*, 48, 223
- Planck Collaboration, Ade, P. A. R., Aghanim, N., et al. 2014, *A&A*, 571, A16
- Press, W. H., & Schechter, P. 1974, *ApJ*, 187, 425
- Rosas-Guevara, Y. M., Bower, R. G., Schaye, J., et al. 2015, *MNRAS*, 454, 1038
- Sawala, T., Frenk, C. S., Fattahi, A., et al. 2016, *MNRAS*, 457, 1931
- Schaye, J., & Dalla Vecchia, C. 2008, *MNRAS*, 383, 1210
- Schaye, J., Crain, R. A., Bower, R. G., et al. 2015, *MNRAS*, 446, 521
- Schneider, A. 2015, *MNRAS*, 451, 3117
- Schneider, A., Smith, R. E., Macciò, A. V., & Moore, B. 2012, *MNRAS*, 424, 684
- Sheth, R. K., Mo, H. J., & Tormen, G. 2001, *MNRAS*, 323, 1
- Shi, X., & Fuller, G. M. 1999, *Physical Review Letters*, 82, 2832
- Springel, V. 2005, *MNRAS*, 364, 1105

- Springel, V., White, S. D. M., Tormen, G., & Kauffmann, G. 2001, MNRAS, 328, 726
- Springel, V., Wang, J., Vogelsberger, M., et al. 2008, MNRAS, 391, 1685
- Turner, M. S., & Wilczek, F. 1991, PhRvL, 66, 5
- van den Bosch, F. C., & Ogiya, G. 2018, MNRAS, 475, 4066
- Viel, M., Becker, G. D., Bolton, J. S., & Haehnelt, M. G. 2013, PhRvD, 88, 043502
- Viel, M., Lesgourgues, J., Haehnelt, M. G., Matarrese, S., & Riotto, A. 2005, PhRvD, 71, 063534
- Wang, J., & White, S. D. M. 2007, MNRAS, 380, 93